Static Micromixer–Coaxial Electrospray Synthesis of Theranostic Lipoplexes

Yun Wu,[†] Lei Li,[†] Yicheng Mao,[†,‡] and Ly James Lee[†,‡,§,*]

[†]Nanoscale Science and Engineering Center for Affordable Nanoengineering of Polymeric Biomedical Devices, The Ohio State University, 174 W 18th Avenue, Columbus, Ohio 43210, United States, [‡]Division of Pharmaceutics, College of Pharmacy, The Ohio State University, 500 W 12th Avenue, Columbus, Ohio 43210, United States, and [§]William G. Lowrie Department of Chemical and Biomolecular Engineering, The Ohio State University, 140 W 19th Avenue, Columbus, Ohio 43210, United States

ABSTRACT

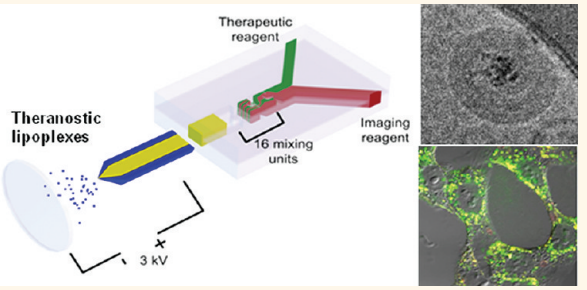

Theranostic lipoplexes are an integrated nanotherapeutic system with diagnostic imaging capability and therapeutic functions. They hold great promise to improve current cancer treatments; however, producing uniform theranostic lipoplexes with multiple components in a reproducible manner is a highly challenging task. Conventional methods, such as bulk mixing, are not able to achieve this goal because of their macroscale and random nature. Here we report a novel technique, called the static micromixer–coaxial electrospray (MCE), to synthesize theranostic lipoplexes in a single step with high reproducibility. In this work, quantum dots (QD605) and Cy5-labeled antisense oligodeoxynucleotides (Cy5-G3139) were chosen as the model imaging reagent and therapeutic drug, respectively. Compared with bulk mixing, QD605/Cy5-G3139-loaded lipoplexes produced by MCE were highly uniform with polydispersity of 0.024 ± 0.006 and mean diameter by volume of 194 ± 15 nm. MCE also showed higher encapsulation efficiency of QD605 and Cy5-G3139. QD605 and Cy5 also formed the Förster resonance energy transfer pair, and thus the cellular uptake and intracellular fate of theranostic lipoplexes could be visualized by flow cytometry and confocal microscopy. The lipoplexes were efficiently delivered to A549 cells (non-small cell lung cancer cell line) and down-regulated the Bcl-2 gene expression by 48 ± 6%.

KEYWORDS: theranostic nanomedicine · lipoplexes · quantum dots · oligonucleotides · static micromixer · coaxial electrospray · Förster resonance energy transfer

Theranostic lipoplex-based nanomedicine with combined imaging, diagnostic, and therapeutic functions has attracted a great deal of interest because of its potential for early cancer detection and cancer therapy. Although the conventional bulk mixing preparation method is simple, the resulting lipoplexes are often nonuniform in size and composition. Producing theranostic lipoplexes in a controlled and affordable process tailored toward the needs of individuals is a highly valuable but challenging task.

Among many technologies, the microfluidic synthesis method has produced uniform lipoplexes in a reproducible manner. For example, Jahn *et al.* used hydrodynamic focusing flow to produce liposomes with sizes less than 200 nm.[1−4] Koh *et al.* developed a multiinlet microfluidic hydrodynamic focusing system to prepare lipopolyplexes loaded with Bcl-2 antisense oligodeoxynucleotide (ODN).[5] Compared to bulk mixing, they found that lipoplexes produced by the microfluidic system had similar multilamellar structures but smaller size and narrower size distribution. These lipoplexes provided a higher level of Bcl-2 antisense ODN uptake and thus led to more efficient down-regulation of the Bcl-2 protein expression. Yu *et al.* also demonstrated that hydrodynamic focusing-based microfluidic synthesis is a simple, affordable, and reproducible method to produce ODN-containing lipoplexes with low polydispersity values.[6] Recently, Valencia *et al.* developed a microfluidic device that combined hydrodynamic flow focusing with passive mixing structures to produce monodisperse lipid–polymer and lipid–quantum dot (QD) nanoparticles in a single step.[7]

Although hydrodynamic focusing-based microfluidic systems are simple and easy to use, the residue of solvents used to dissolve lipids and lipophilic components, such as isopropyl alcohol used by Jahn *et al.* and tetrahydrofuran used by Valencia *et al.*, may limit the applications of lipoplexes. Electrospray, on the other hand, is a microfluidics-based aerosol generation method that uses electrical forces to disperse liquids into fine particles. The solvents used in the process can evaporate quickly due to the large surface area of the tiny airborne droplets, and therefore, this method can minimize the

* Address correspondence to lee.31@osu.edu.

Received for review November 6, 2011 and accepted February 9, 2012.

Published online February 10, 2012
10.1021/nn204300s

solvent toxicity issue. Electrospray is well-known for its critical application in the electrospray ionization mass spectrometry, an analytical technique developed by the 2002 chemistry Nobel Prize winner, Dr. John B. Fenn.[8] During the past two decades, electrospray has been widely used to produce micro- and nanoparticles.[9−11] Furthermore, electrospray is able to produce uniform nanoparticles without changing the biological activity of nucleic acids,[12−14] cells,[15] proteins,[16,17] and lipids.[12,18] Recently, we developed a coaxial electrospray system that successfully produced monodisperse ODN-containing lipoplexes.[12] In the coaxial electrospray setup, a concentric needle was used to bring two solutions together, and an electric field was applied to disperse the liquid into monodisperse, fine droplets. The solvent evaporated quickly, leading to a unilamellar structure in contrast with the multilamellar structure of lipoplexes produced by the hydrodynamic focusing-based microfluidics and conventional bulk mixing methods.

The aforementioned methods focus mostly on nanoparticles with single modality, either therapeutic or imaging function. In this work, we present a novel static micromixer−coaxial electrospray (MCE) system, which combines the advantages of static micromixer and coaxial electrospray to produce theranostic lipoplexes with both imaging and therapeutic functions in a single step. The static micromixer is used to bring together the imaging reagent stream and the therapeutic reagent stream at the microscale and further reduce the stream width to the nanoscale (*i.e.*, greatly increase the interfacial contact area between the two streams) by the repeated stretching−folding function of the static mixing units. The multilayered mixture of imaging reagent and therapeutic reagent then flows through the inner needle of the coaxial electrospray system. The lipids are dissolved in ethanol and flow through the outer needle of the coaxial electrospray system. A high electric field is applied to disperse the entire imaging reagent/therapeutic reagent/lipids mixture into fine droplets. After the quick evaporation of ethanol, theranostic lipolexes are formed. In this study, we chose QD605 as the model imaging reagent and Cy5-labeled antisense ODN, Cy5-G3139, as the model therapeutic reagent. QD605 and Cy5 form a Förster resonance energy transfer (FRET) pair, providing a useful tool to study the cellular uptake and intracellular fate of theranostic lipoplexes.

RESULTS AND DISCUSSION

Device Design and Fabrication. Figure 1 shows the MCE device used in this work. The device consists of two parts, a static micromixer and a coaxial electrospray system. Microinjection molding was chosen to fabricate this static micromixer.[19,20] In order to reduce the cost and achieve mass production, two identical parts were designed for the static micromixer, and therefore, only one mold is needed for the device fabrication. For

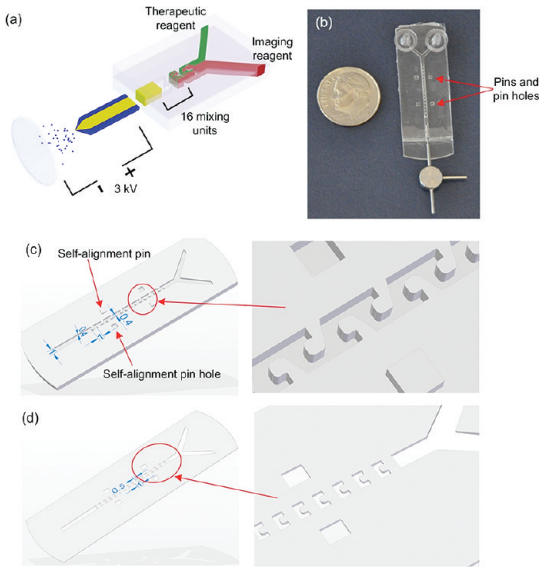

Figure 1. Schematic diagram (a) and the image (b) of the static micromixer−coaxial electrospray device used for theranostic lipoplexes synthesis. Schematic diagrams of the static micromixer (c) and the dividing film (d) (unit: mm).

microinjection molding, all of the features were designed to be perpendicular to the bottom surface for simplicity. The mold was machined on a micromilling machine with a 200 μm diameter flat end mill. The material of the mold was aluminum 6061, and the diameter of the mold was 40 mm. The injection molding process was performed on a 30 ton microinjection molding machine (Sodick Plustech), and the material was polymethyl methacrylate (PMMA) for its high optical clarity. Most microfluidic devices are fabricated using polydimethylsiloxane (PDMS) and the soft lithography process. Although PDMS-based devices have the advantages of simplicity, good biocompatibility, and easy sealing with glass and silicon, the fabrication method is slow and costly. We used a widely used plastic, PMMA, and the microinjection molding method to substantially reduce the fabrication time (less than 1 min for one mixer).

A divider, which is parallel to the bottom surface at the entrance of each mixing unit, was fabricated from a 100 μm thick PMMA sheet (shinkolite, Mitsubishi Rayon) using micromilling (Figure 1d). After molding, the divider sheet was placed between the top and bottom mixer parts with good alignment (by utilizing the alignment pins/pin holes), and the three pieces were assembled by thermal bonding. By using thermal bonding, micromixers and the divider sheet can be well sealed and the resulting bonding can stand high pressure and flow rates.

At the outlet of the static micromixer, a concentric needle was attached to perform coaxial electrospray to produce lipoplexes. The concentric needle had a 27 gauge inner needle and a 20 gauge outer needle. The inner needle was connected to the outlet of the

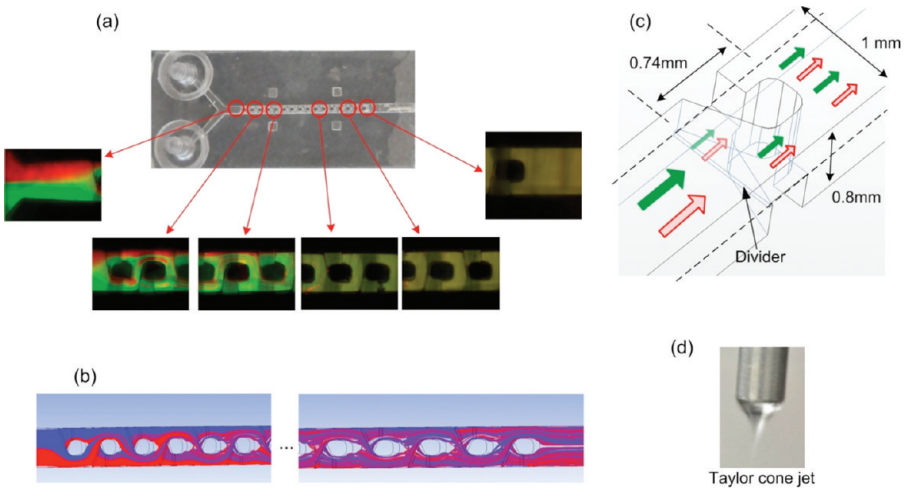

Figure 2. Experimental (a) and simulated (b) flow patterns of the static micromixer. (c) Structure of one mixing unit of the static micromixer. Theoretically, the split-and-recombination structure can double the number of layers of the incoming flow and at the same time halve the width of each layer. (d) Taylor cone jet mode of coaxial electrospray, in which monodisperse lipoplexes were produced.

static micromixer using the UV curing glue. A 20 gauge three-way tubing connector was used as the outer needle. A positive high voltage was applied to the outer needle to break the liquid into monodisperse nanoparticles.

Flow Pattern of the MCE Device. In this work, a static micromixer was used to uniformly mix multiple fluids/components from the micro- to nanoscale. Figure 2a shows the multiple lamination flow pattern inside the micromixer of two liquids labeled with rhodamine (red fluorescence) and fluorescein (green fluorescence). The multiple lamination structure was clearly seen at the outlet of the static micromixer. CFD (computer fluid dynamics) simulation was carried out in the design process by using a commercial program ANSYS CFX to optimize the structures of the micromixer. In the simulation, diffusion was ignored to better demonstrate the mixing performance caused by multiple lamination structures. Particle tracking was used in simulation to show the flow pattern inside the static micromixer (Figure 2b). The experimental flow pattern agreed well with the simulated flow pattern.

The formation of multiple laminations inside the static micromixer can be explained by the classical split-and-recombination (SAR) theory. The designed device consists of 16 identical mixing units. Figure 2c shows the structure of one unit as well as the mixing principle. The incoming flow consists of two laminar streams (indicated as the green and red arrows) before entering the mixing units. At the front end of the mixing unit, the incoming flow is divided into two subflows, and each subflow contains the same amount of the two incoming streams. At the back side of the mixing unit, the two subflows are recombined into one flow. As a result, the number of the layers in the flow is doubled and the width of each layer is halved after one mixing unit. The repeated stretching-and-folding function of the mixing units can reduce the width of the flow stream to as small as several nanometers in the static micromixer. Theoretically, at the outlet of the micromixer, the obtained number of striations is $N_s = 2 \times 2^m$, where m is the number of mixing units. Since there are 16 mixing units in our design and the initial stream width is 500 μm, thus the final width of each stream could be 7.6 nm at the outlet of the micromixer. Compared with the hydrodynamic focusing method which has only one interfacial contact surface, the multiple lamination structure induced in the static micromixer can provide much larger contact surface between the incoming reagent streams and thus provide better mixing.

The mixture of imaging reagent (QD605) and therapeutic reagent (Cy5-G3139) then flowed through the inner needle of the coaxial electrospray apparatus. The lipid mixture (DOTAP/EggPC/DSPE-PEG = 30:69:1 molar ratio) was dissolved in ethanol and fed though the outer needle. With a positive voltage applied (~3 kV) to the outer needle, a Taylor cone jet (Figure 2d) was formed at the end of the needle when the electrical stress overcame the surface tension of the liquid. The jet was not stable and easily broke into tiny droplets. With quick evaporation of ethanol due to the huge surface areas of tiny droplets, QD605/Cy5-G3139-loaded lipoplex aerosol nanoparticles were formed rapidly.

Size Distribution, Structure, and Zeta-Potential of QD605/Cy5-G3139-Loaded Lipoplexes. Figure 3 shows the typical size distributions of QD605/Cy5-G3139-loaded lipoplexes prepared by MCE (Figure 3a) and bulk mixing (Figure 3b). For lipoplexes produced by MCE, the mean diameter by volume was 194 ± 15 nm, the polydispersity was 0.024 ± 0.006, and the zeta-potential was 20.52 ± 1.28 mV. For lipoplexes produced by bulk mixing, the mean diameter by volume was 85.2 ± 10.6 nm, the polydispersity was 0.16 ± 0.04, and the

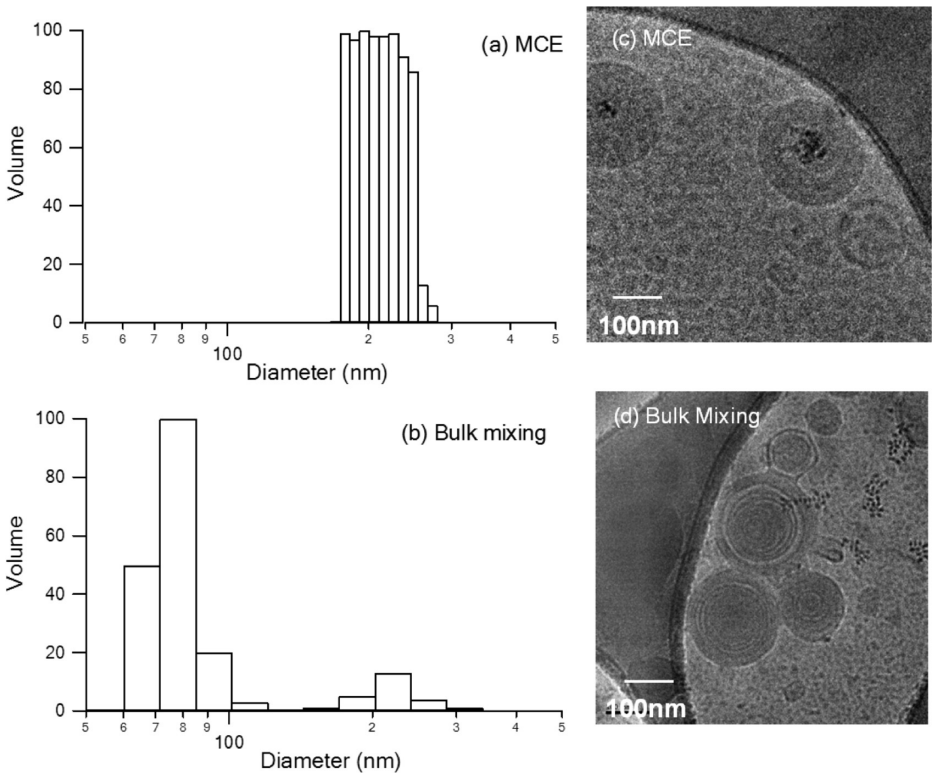

Figure 3. Typical size distributions and structures of QD605/Cy5-G3139-loaded lipoplexes produced by MCE (a,c) and bulk mixing (b,d). QD605/Cy5-G3139-loaded lipoplexes produced by MCE were monodisperse and had a unilamellar structure with QD605 successfully encapsulated inside the nanoparticle, while those prepared by bulk mixing were polydisperse with most QD605 left outside of nanoparticles.

zeta-potential was 13.28 ± 0.94 mV. Cryo-TEM images showed that the QD605/Cy5-G3139-loaded lipoplexes produced by MCE were monodisperse and had a unilamellar structure with QD605 successfully encapsulated inside the nanoparticles (Figure 3c), while those prepared by bulk mixing were polydisperse with most of QD605 left outside of the nanoparticles (Figure 3d). The physicochemical properties of lipoplexes, such as reagent loading efficiency, size, shape, surface charge, and targeting ligands, are important factors in determining the successful clinical translation of theranostic lipoplexes.[21] The lipoplexes produced by MCE and bulk mixing have appropriate size and surface charge for both *in vitro* and *in vivo* applications,[22,23] but as theranostic nanomedicine, lipoplexes produced *via* MCE showed higher loading efficiency of the imaging reagent than bulk mixing.

Fluorospectrum of QD605/Cy5-G3139-Loaded Lipoplexes. Förster resonance energy transfer (FRET) is a useful tool in evaluating molecular dynamics at the nanometer scale.[24,25] As shown in Figure 4a, QD605 (excitation peak at 405 nm, emission peak at 605 nm) and Cy5-G3139 (excitation peak at 650 nm, emission peak at 670 nm) formed a FRET pair. The quantum yield of QD605 used in this work is ~0.65 (provided by eBioscience Inc.), and the Förster distance for the donor–acceptor pair was 72.5 Å. When the energy donor (QD605) is close to the energy acceptor (Cy5),

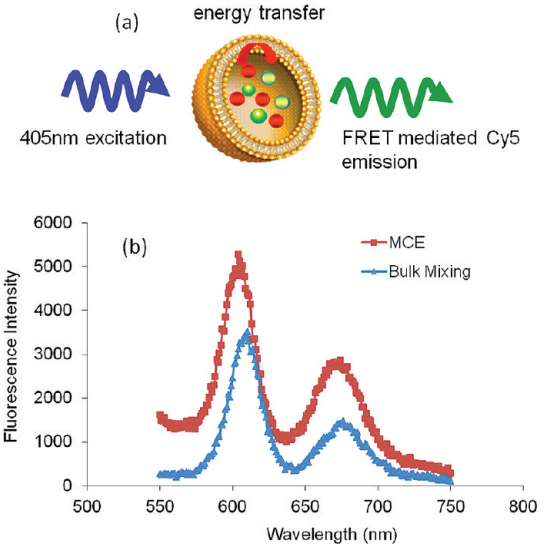

Figure 4. (a) QD-mediated Föster resonance energy transfer (QD-FRET) of QD605/Cy5-G3139-loaded lipoplexes and (b) typical fluorospectra of lipoplexes produced by MCE and bulk mixing upon excitation at 405 nm.

the fluorescence energy of QD605 will transfer to Cy5 and thus the emission of Cy5 fluorescence is observed upon excitation at 405 nm. When the distance between QD605 and Cy5 is larger than the Förster distance, the Cy5 fluorescence will not be observed upon excitation at 405 nm. The QD-mediated FRET

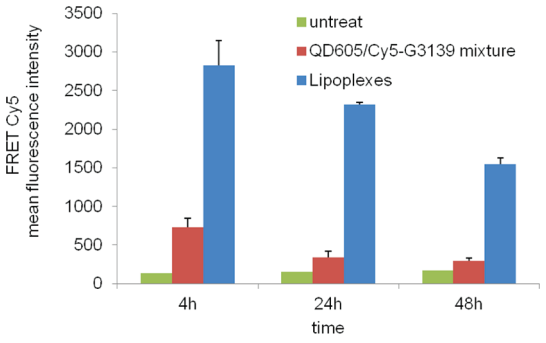

Figure 5. Flow cytometry analysis. QD605-mediated FRET Cy5 mean fluorescence intensity 4, 24, and 48 h after A549 cells were transfected by the mixture of free QD605 and Cy5-G3139, and the QD605/Cy5-G3139-loaded lipoplexes produced by MCE.

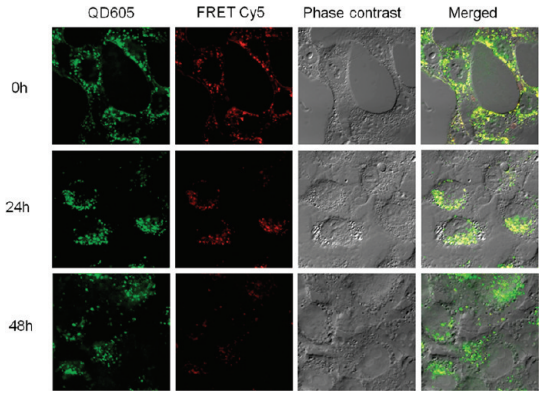

Figure 6. Confocal microscopy analysis at 4, 24, and 48 h after A549 cells were transfected by QD605/Cy5-G3139-loaded lipoplexes produced by MCE. DIC: differential interference contrast.

provides a tool to study the intracellular fate of the theranostic lipoplexes. Figures 4b shows typical fluorospectra of QD605/Cy5-G3139-loaded lipoplexes produced by MCE and bulk mixing upon excitation at 405 nm. At the same QD605 concentration of 6 nM and Cy5-G3139 concentration of 7.2 μg/μL, the estimated FRET efficiency for lipoplexes prepared by MCE was 0.55 and those prepared by bulk mixing was 0.41. Higher FRET efficiency of lipoplexes produced by MCE suggested that MCE had better encapsulation efficiency of QD605 and Cy5-G3139 than bulk mixing.

Cellular Uptake and Intracellular Fate of QD605/Cy5-G3139-Loaded Lipoplexes. The cellular uptake of QD605/Cy5-G3139-loaded lipoplexes in A549 cells was first evaluated by flow cytometry (Figure 5). Compared with untreated cells and cells transfected with the mixture of free QD605 and Cy5-G3139, much higher FRET-mediated Cy5 fluorescence was observed with the cells transfected by QD605/Cy5-G3139-loaded lipoplexes at 4, 24, and 48 h post-transfection, indicating that lipoplexes are a good nanocarrier system.

The intracellular fate of QD605/Cy5-G3139-loaded lipoplexes in A549 cells was then investigated by laser scanning confocal microscopy (Figure 6). Results showed that lipoplexes accumulated around the edge of the cells and strong FRET-mediated Cy5 signal was observed at 4 h post-transfection. The colocalization of QD605 (pseudocolored in green) and Cy5 (pseudocolored in red) suggested that the nanoparticles were still intact and were not disassembled. Twenty-four hours post-transfection, the lipoplexes moved toward the center of the cells and the FRET-mediated Cy5 signal decreased, indicating the breakup of lipoplexes and the dissociation of QD605 and Cy5-G3139. Forty-eight hours post-transfection, most lipoplexes broke up and QD605 dissociated from Cy5-G3139, indicating the successful release of Cy5-G3139 into the cytoplasm.

MATLAB software was used to further analyze the colocalization of QD605 and Cy5-G3139. As shown in Figure S1 in the Supporting Information, three representative lines were drawn on each image and the corresponding fluorescence intensity of QD605 (green curve) and FRET-mediated Cy5-G3139 (red curve) was plotted against its position on the image. At 0 h, the red curve followed the green curve very well, and the fluorescence intensity of FRET-mediated Cy5-G3139 was also high, which suggested the colocalization of QD605 and Cy5-G3139. At 24 h post-transfection, the fluorescence intensity of FRET-mediated Cy5-G3139 decreased. At some locations, only strong fluorescence of QD605 was observed with limited or no fluorescence from FRET-mediated Cy5-G3139, suggesting that lipoplexes broke up and the QD605 was dissociated from Cy5-G3139. At 48 h post-transfection, the fluorescence intensity of QD605 was still strong, but the fluorescence intensity of FRET-mediated Cy5-G3139 decreased significantly, indicating the further dissociation of QD605 from Cy5-G3139.

Since the decrease of the FRET-mediated Cy5 signal may also be caused by the degradation of Cy5,[26] a control experiment was carried out to determine the extent of degradation of the Cy5 dye 48 h post-transfection. A549 cells were transfected with Cy5-G3139 without QD605. The fluorescence intensity of Cy5 decreased ~26% over 48 h time period (data not shown). However, the FRET-mediated Cy5 fluorescence intensity decreased ~45% over the same time period, as shown in Figure 5, implying that our FRET measurements reflected both dye degradation and lipoplexes breakup. The successful down-regulation of Bcl-2 gene expression shown later in this paper confirms that the breakup of lipoplexes to release Cy5-G3139 in the cytoplasm did occur in our study.

Bcl-2 Down-Regulation by QD605/Cy5-G3139-Loaded Lipoplexes. The biological activities of QD605/Cy5-G3139-loaded lipoplex nanoparticles were evaluated in A549 cell line 48 h after transfection. G3139 is specially designed to bind the first six codons of the human Bcl-2 mRNA and thus inhibits the Bcl-2 expression, providing a way to decrease the resistance of cancer cells to chemotherapy.[12] As shown in Figure 7, Bcl-2

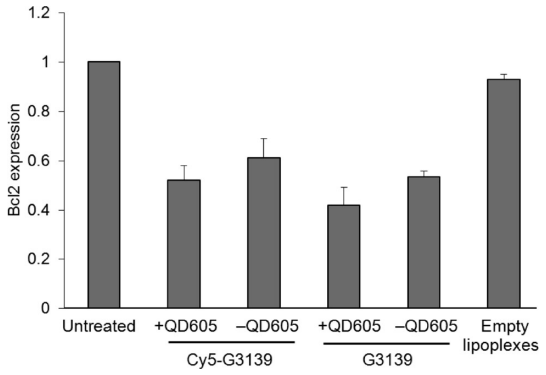

Figure 7. Bcl-2 down-regulation by lipoplexes produced by MCE. QD605 and Cy5 labeling did not affect the biological activity of lipoplexes.

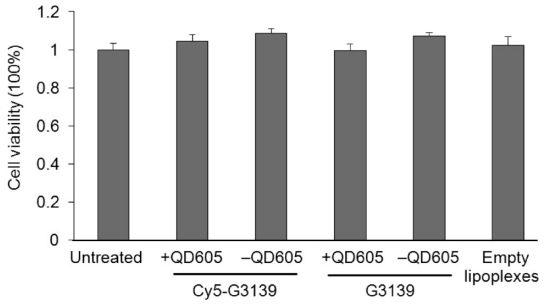

Figure 8. Cytotoxicity of lipoplexes in A549 cells. Compard with untreated cells, QD605/Cy5-G3139-loaded lipoplexes and nonlabeled counterparts showed little cytotoxicity.

expression was successfully down-regulated by 48 ± 6% when transfected with QD605/Cy5-G3139-loaded lipoplexes at G3139 concentration of 1 μM. Compared with the nonlabeled counterparts, the addition of QD605 did not affect the biological activities of lipoplexes and the Cy5 labeling had little effect on the biological function of G3139.

Cytotoxicity of QD605/Cy5-G3139-Loaded Lipoplexes. The cytotoxicity of QD605/Cy5-G3139-loaded lipoplexes was evaluated in A549 cell line 48 h post-transfection. As shown in Figure 8, compared with untreated cells, little cell viability decrease was observed in cells treated with QD605/Cy5-G3139-loaded lipoplexes and the nonlabeled counterparts at the G3139 concentration of 1 μM.

DISCUSSION

Many theranostic nanoparticle systems have been developed using different imaging modalities, each with their own advantages and disadvantages. They include drug conjugates, dendrimers, micelles, core–shell structures, micro/nanobubbles, carbon nanotubes, and complexes.[23,27,28] Compared to free drugs, drug conjugates have improved therapeutic efficacy by decreasing the toxicity and increasing the circulation time. When imaging modality is incorporated in the nanocarrier, it is often difficult to achieve both high drug loading and reliable production. Dendrimers hold great promise as successful drug and imaging agent carrier systems in a number of preclinical studies, but toxicity and off-target effects need to be overcome. Micelles are easy to produce, can encapsulate hydrophobic drugs, and have demonstrated therapeutic success in clinical and preclinical studies, but the stability of the micelles is the major limitation. Core–shell structured nanoparticles made with materials such as quantum dots, magnetic nanoparticles, and gold nanoparticles offer good physiological stability, controlled drug release, and can even serve as imaging or therapeutic reagents depending on their composition, size, and shape. However, intrinsic limitations such as toxicity, rapid clearance, and poor biodistribution are the major barriers in the development of core–shell structured nanoparticles. Micro/nanobubbles have been developed as a contrast agent for ultrasound imaging, but their therapeutic function requires further evaluation. Carbon nanotubes (CNTs) are relatively new carrier systems. Although many studies have shown that CNTs are good theranostic systems *in vitro*, the cytotoxicity and biodegradation route *in vivo* are the major concerns. Complexes, including lipoplexes and polyplexes, are versatile and tunable carrier systems, which can efficiently load drugs and imaging agents, incorporate targeting molecules, and provide long circulation time and good tumor accumulation. However, production complexity and toxicity are the major challenges when incorporating new materials in lipoplexes or adding new chemistry to polyplexes. During clinical transition, it is critical to have a reliable production process. In this work, we demonstrated that our MCE device is able to produce uniform theranostic lipoplexes in a single step with high reproducibility. Theranostic lipoplexes also showed good therapeutic and imaging ability with little toxicity. The MCE device will benefit the development of theranostic complexes and facilitate clinical transition.

CONCLUSIONS

A MCE device was developed to produce QD605/Cy5-G3139-loaded theranostic lipoplexes in a well-controlled manner. Compared with the conventional bulk mixing method, the lipoplexes produced by MCE were more monodisperse with a diameter of ~194 nm and a polydispersity of ~0.024. Both cryo-TEM images and fluorospectra showed that MCE provided higher encapsulation efficiency of QD605 and Cy5-G3139. The theranostic lipoplexes successfully delivered the imaging reagent (QD605) and therapeutic reagent (Cy5-G3139) to A549 cells. The cellular uptake and intracellular fate of lipoplexes were visualized by flow cytometry and confocal microscopy. Successful dissociation of lipoplex nanoparticles inside the cytoplasm

led to ~48% down-regulation of the target gene, Bcl-2. Since electrospray is an aerosol generation technique, the MCE device may have great potential to produce theranostic nanoparticles for pulmonary delivery of nucleic acid drugs in lung disease and cancer treatment in the future.

MATERIALS AND METHODS

Materials. QD605-amine was purchased from eBioscience, Inc. (93-6366-33). The Cy5-labeled ODN (Cy5-G3139, 5′-Cy5-TCT CCC AGC GTG CGC CAT-3′) was custom synthesized by Alpha DNA, Inc. (Montreal, Canada). 2,3-Dioleoyloxypropyltrimethylammonium chloride (DOTAP) was purchased from Genzyme Inc. (LP-04-117). Egg phosphatidylcholine (EggPC) and methoxypolyethylene glycol (MW ≈ 2000 Da) distearoyl phosphatidylethanolamine (PEG-DSPE) were obtained from Lipoid (Newark, NJ). Two-hundred proof ethanol was purchased from Pharmco-Aaper (E200GP), and 1× PBS was purchased from Fisher Scientific (BP3994).

Preparation of QD605/Cy5-G3139-Loaded Lipoplexes *via* MCE. As shown in Figure 1a, 0.2 μM QD605-amine and 0.24 μg/μL Cy5-G3139 were brought together through two inlets of the static micromixer at same flow rate of 10 μL/min, where QD605 and Cy5-G3139 were well mixed at the outlet. The mixture of QD605 and Cy5-G3139 was then fed through the inner needle of the coaxial electrospray apparatus. A lipid mixture (DOTAP/EggPC/DSPE-PEG = 30:69:1 molar ratio) was dissolved in ethanol at concentration of 1.5 μg/μL and fed though the outer needle at the flow rate of 20 μL/min. A positive voltage (~3 kV) was applied to the outer needle to break the liquid into tiny droplets. The ethanol evaporated quickly, and QD605/Cy5-G3139-loaded lipoplexes were formed at the lipid/Cy5-G3139 mass ratio of 12.5. Lipoplexes were captured in 1× PBS solution and sterilized by filtering through 0.2 μm PVDF filter before use.

QD605/Cy5-G3139-loaded lipoplexes were also prepared by bulk mixing. Briefly, 0.2 μM QD605 was first mixed with 0.24 μg/μL Cy5-G3139. Then the 1.5 μg/μL lipid mixture was added to achieve 50% ethanol and 50% aqueous in the final mixture with the lipid/Cy5-G3139 mass ratio of 12.5. The mixture was dialyzed against 1× PBS overnight to remove ethanol and form QD605/Cy5-G3139-loaded lipoplexes.

Size Distribution and Zeta-Potential Measurement. The size distribution of QD605/Cy5-G3139-loaded lipoplexes was measured using dynamic light scattering (DLS) (Brookhaven Instruments Corporation, Holtsville, NY, BI 200SM). The wavelength of the laser was 632.8 nm, and the detection angle was 90°. All measurements were carried out at 20 °C with 1× PBS as the dilution buffer. The size distributions of three batches of QD605/Cy5-G3139-loaded lipoplexes prepared independently were measured at 20 °C. The mean diameter by volume ± standard deviation was reported.

The zeta-potential of QD605/Cy5-G3139-loaded lipoplexes was measured by a ZetaPALS zeta-potential analyzer (Brookhaven Instruments Corporation, Holtsville, NY). Three batches of independently prepared lipoplexes were diluted in 1× PBS buffer. Three measurements, each consisting of 5 runs, were performed at 20 °C. The Smoluchowski model was used to calculate the zeta-potential, and the mean ± standard deviation was reported.

Cryo-Transmission Electron Microscopy (Cryo-TEM). One drop of QD605/Cy5-G3139-loaded lipoplexes solution was placed on a lacey Formvar/carbon film coated Cu TEM grid using a micropipet. The excess fluid on the grid surface was removed by blotting the surface with a filter paper. The grid was then plunged into a small vessel of liquid ethane that was located in a larger liquid nitrogen vessel to vitrify the water film on the grid and to avoid water crystallization.

The quenched sample grid was transferred into the grid box that was also stored in liquid nitrogen. The grid was transferred into a Gatan cryo-transfer system filled with liquid nitrogen and loaded onto a cryo-TEM stage. The cryo stage was loaded into the TEM (FEI Tecnai G2 Spirit BioTWIN), and the images were taken at temperatures below −170 °C. The digital images were recorded using a Gatan CCD camera.

Fluorospectrophotometry. QD605/Cy5-G3139-loaded lipoplexes prepared by MCE and bulk mixing were diluted in 1× PBS buffer to achieve QD605 concentration of 6 nM. The samples were then added into plastic methacrylate cuvettes (Fisher Scientific, Pittsburgh, PA). Fluorescence emission spectra (550−750 nm) of lipoplexes upon excitation at 405 nm were scanned by a spectrofluorometer (PTI Inc.).

A549 Cell Culture. A549 cells (non-small cell lung cancer cell line), obtained from the American Type Culture Collection (ATCC) (Manassas, VA), were routinely cultured in a 75 cm^2 T flask containing 15 mL of RPMI 1640 media supplemented with 10% fetal bovine serum (FBS, Gibco 160000). The cells were seeded into 75 cm^2 T flasks at a concentration of 1×10^5 viable cells/mL and incubated at 37 °C in a humidified atmosphere containing 5% CO_2. The cells were subcultured every 3 days.

Transfection Studies of QD605/Cy5-G3139 Lipoplexes. A549 cells were seeded at 2×10^5 viable cells/well in 6-well plates containing 2 mL of culture medium supplemented with 10% FBS, or at 4×10^4 viable cells/well on cover glasses (Fisher Scientific, 12-545-82) in 24-well plates containing 0.4 mL of culture medium supplemented with 10% FBS. The cells were incubated at 37 °C in a humidified atmosphere containing 5% CO_2 overnight. Then the culture medium was replaced with the medium containing no FBS. QD605/Cy5-G3139-loaded lipoplexes, the nonlabeled counterparts, and empty lipoplexes were then added into the medium at the Cy5-G3139 concentration of 1 μM and QD605 concentration of 5 nM. The cells were incubated at 37 °C for 4 h, and the transfection process was stopped by transferring cells into fresh culture medium supplemented with 10% FBS (2 mL for 6-well plates and 0.4 mL for 24-well plates). All transfection experiments were performed in triplicate.

Cellular Uptake and Intracellular Fate of the QD605/Cy5-G3139-Loaded Lipoplexes. The cellular uptake and intracellular fate of the QD605/Cy5-G3139-loaded lipoplexes were examined by flow cytometry (BD LSR II) and laser scanning confocal microscopy (Olympus FV1000). In flow cytometry experiments, A549 cells were cultured in 6-well plates and transfected with QD605/Cy5-G3139-loaded lipoplexes following the aforementioned transfection procedure. The cells were harvested 4, 24, and 48 h after the addition of lipoplexes. When preparing the samples, the cells were first detached from culture plates using 0.25% trypsin, washed with PBS twice, and fixed using 4% paraformaldehyde. The fluorescence signals of QD605 and FRET-mediated Cy5 were observed in the QD605 and PE-Cy5 channels, respectively. Ten thousand events were collected for each sample, and the average results of three replicates were reported.

In confocal microscopy experiments, A549 cells were cultured on cover glasses in 24-well plates and treated with QD605/Cy5-G3139-loaded lipoplexes following the aforementioned transfection procedure. Cells were harvested 4, 24, and 48 h after the addition of nanoparticles. To prepare the samples, cells were washed with 1× PBS twice and fixed with 4% paraformaldehyde at room temperature for 1 h. The cells were then washed with PBS twice and mounted on glass slides for confocal microscopy analysis. The excitation wavelength was set at 405 nm, and the fluorescence signals of QD605 and FRET Cy5 were observed in the QD605 (dichroic mirror 560−620 nm) and Cy5 (dichroic mirror 655−755 nm) channels, respectively.

Quantification of Bcl-2 mRNA Expression in A549 Cells by Quantitative Real-Time PCR (qRT-PCR). Forty-eight hours post-transfection, the cells were washed with cold 1× PBS twice and then treated with 1 mL of TRIzol (Invitrogen). Total RNA was extracted by adding chloroform. The total RNA was further purified by isopropyl alcohol precipitation and washed by 70% ethanol. The total RNA was transcribed into cDNA using the first-strand cDNA synthesis kit (Invitrogen 18080051). The resulting cDNA was amplified by qRT-PCR (Invitrogen, Taqman Assay Hs00608023_m1). Relative

gene expression values were determined by the ΔΔCT method. Bcl-2 expression was normalized to GAPDH (Invitrogen, Taqman Assay Hs02758991_g1), which was the endogenous reference in the corresponding samples, and relative to the untreated control cells.

Cytotoxicity of QD605/Cy5-G3139-Loaded Lipoplexes in A549 Cells. The cytotoxicity of QD605/Cy5-G3139-loaded lipoplexes, the non-labeled counterparts, and empty lipoplexes was evaluated using alamarBlue assay (Invitrogen, A13262). Forty-eight hours post-transfection, the cells were incubated with fresh culture medium containing 10% alamarBlue for 2 h at 37 °C in a humidified, 5% CO_2 atmosphere, protected from light. The fluorescence intensity was read at an emission wavelength of 590 nm under the excitation wavelength of 570 nm using a microplate reader (GENios Pro, Tecan, USA).

Conflict of Interest: The authors declare no competing financial interest.

Acknowledgment. This work was supported by the National Science Foundation under Grant No. EEC-0425626.

Supporting Information Available: Figures depicting the colocalization analysis of QD605 and Cy5-G3139 at 0, 24, and 48 h after A549 cells were transfected by QD605/Cy5-G3139-loaded lipoplexes produced *via* MCE. This material is available free of charge *via* the Internet at http://pubs.acs.org.

REFERENCES AND NOTES

1. Jahn, A.; Vreeland, W. N.; Gaitan, M.; Locascio, L. E. Controlled Vesicle Self-Assembly in Microfluidic Channels with Hydrodynamic Focusing. *J. Am. Chem. Soc.* **2004**, *126*, 2674–2675.
2. Jahn, A.; Vreeland, W. N.; DeVoe, D. L.; Locascio, L. E.; Gaitan, M. Microfluidic Directed Formation of Liposomes of Controlled Size. *Langmuir* **2007**, *23*, 6289–6293.
3. Jahn, A.; Reiner, J. E.; Vreeland, W. N.; DeVoe, D. L.; Locascio, L. E.; Gaitan, M. Preparation of Nanoparticles by Continuous-Flow Microfluidics. *J. Nanopart. Res.* **2008**, *10*, 925–934.
4. Jahn, A.; Stavis, S. M.; Hong, J. S.; Vreeland, W. N.; DeVoe, D. L.; Gaitan, M. Microfluidic Mixing and the Formation of Nanoscale Lipid Vesicles. *ACS Nano* **2010**, *4*, 2077–2087.
5. Koh, C. G.; Zhang, X.; Liu, S.; Golan, S.; Yu, B.; Yang, X.; Guan, J.; Jin, Y.; Talmon, Y.; Muthusamy, N.; *et al.* Delivery of Antisense Oligodeoxyribonucleotide Lipopolyplex Nanoparticles Assembled by Microfluidic Hydrodynamic Focusing. *J. Controlled Release* **2010**, *141*, 62–69.
6. Yu, B.; Zhu, J.; Xue, W.; Wu, Y.; Huang, X.; Lee, L. J.; Lee, R. J. Microfluidic Assembly of Lipid-Based Oligonucleotide Nanoparticles. *Anticancer Res.* **2011**, *31*, 771–776.
7. Valencia, P. M.; Basto, P. A.; Zhang, L.; Rhee, M.; Langer, R.; Farokhzad, O. C.; Karnik, R. Single-Step Assembly of Homogenous Lipid-Polymeric and Lipid-Quantum Dot Nanoparticles Enabled by Microfluidic Rapid Mixing. *ACS Nano* **2010**, *4*, 1671–1679.
8. Fenn, J. B.; Mann, M.; Meng, C. K.; Wong, S. F.; Whitehouse, C. M. Electrospray Ionization for Mass Spectrometry of Large Biomolecules. *Science* **1989**, *246*, 64–71.
9. Salata, V. Tools of Nanotechnology: Electrospray. *Curr. Nanosci.* **2005**, *1*, 25–33.
10. Yurteri, C. U.; Hartman, R. P. A; Marijnissen, J. C. M. Producing Pharmaceutical Particles *via* Electrospraying with an Emphasis on Nano and Nano Structured Particles - A Review. *KONA Powder Part. J.* **2010**, *28*, 91–115.
11. Jaworek, A.; Sobczyk, A. T. Electrospraying Route to Nanotechnology: An Overview. *J. Electrostat.* **2008**, *66*, 197–219.
12. Wu, Y.; Yu, B.; Jackson, A.; Zha, W.; Lee, L. J.; Wyslouzil, B. E. Coaxial Electrohydrodynamic Spraying: A Novel One-Step Technique To Prepare Oligodeoxynucleotide Encapsulated Lipoplex Nanoparticles. *Mol. Pharmaceutics* **2009**, *6*, 1371–1379.
13. Wu, Y.; Fei, Z.; Lee, L. J.; Wyslouzil, B. E. Electrohydrodynamic Spraying of DNA/Polyethylenimine Polyplexes for Nonviral Gene Delivery. *Biotechnol. Bioeng.* **2009**, *105*, 834–841.
14. Chen, D. R.; Wendt, C. H.; Pui, D. Y. H. A Novel Approach for Introducing Bio-materials into Cells. *J. Nanopart. Res.* **2000**, *2*, 133–139.
15. Jayasinghe, S, N.; Qureshi, A, N.; Eagles, P. A. M. Electrohydrodynamic Jet Processing: An Advanced Electric-Field-Driven Jetting Phenomenon for Processing Living Cells. *Small* **2006**, *2*, 216–219.
16. Pareta, R.; Brindley, A.; Edirisinghe, M. J.; Jayasinghe, S. N.; Lukinska, Z. B. Electrohydrodynamic Atomization of Protein (Bovine Serum Albumin). *J. Mater. Sci: Mater. Med.* **2005**, *16*, 919–925.
17. Xie, J.; Wang, C. Encapsulation of Proteins in Biodegradable Polymeric Microparticles Using Electrospray in the Taylor Cone-jet Mode. *Biotechnol. Bioeng.* **2007**, *97*, 1278–1290.
18. Wu, Y.; Chalmers, J. J.; Wyslouzil, B. E. The Use of Electrohydrodynamic Spraying To Disperse Hydrophobic Compounds in Aqueous Media. *Aerosol Sci. Technol.* **2009**, *43*, 902–910.
19. Li, L.; Lee, L. J.; Castro, J. M.; Yi, A. Y. Improving Mixing Efficiency of a Polymer Micromixer by Use of a Plastic Shim Divider. *J. Micromech. Microeng.* **2010**, *20*, 035012.
20. Li, L.; Yang, C.; Shi, H.; Liao, W. C.; Huang, H.; Lee, L. J.; Castro, J. M.; Yi, A. Y. Design and Fabrication of an Affordable Polymer Micromixer for Medical and Biomedical Applications. *Polym. Eng. Sci.* **2010**, *50*, 1594–1604.
21. Farokhzad, O. C.; Langer, R. Nanomedicine: Developing Smarter Therapeutic and Diagnostic Modalities. *Adv. Drug Delivery Rev.* **2006**, *58*, 1456–1459.
22. Hillaireau, H.; Couvreur, P. Nanocarriers' Entry into the Cell: Relevance to Drug Delivery. *Cell. Mol. Life Sci.* **2009**, *66*, 2873–2896.
23. Peer, D.; Karp, J. M.; Hong, S.; Farokhzad, O. C.; Margalit, R.; Langer, R. Nanocarriers as an Emerging Platform for Cancer Therapy. *Nat. Nanotechnol.* **2007**, *2*, 751–760.
24. Medintz, I. L.; Mattoussi, H. Quantum Dot-Based Resonance Energy Transfer and Its Growing Application in Biology. *Phys. Chem. Chem. Phys.* **2009**, *11*, 17–45.
25. Michalet, X.; Pinaud, F. F.; Bentolila, L. A.; Tsay, J. M.; Doose, S.; Li, J. J.; Sundaresan, G.; Wu, A. M.; Gambhir, S. S.; Weiss, S. Quantum Dots for Live Cells, *In Vivo* Imaging, and Diagnostics. *Science* **2005**, *307*, 538–544.
26. Delehanty, J. B.; Bradburne, C. E.; Boeneman, K.; Susumu, K; Farrell, D.; Mei, B, C.; Blanco-Canosa, J. B.; Dawson, G.; Dawson, P. E.; Mattoussi, H.; *et al.* Delivering Quantum Dot-Peptide Bioconjugates to the Cellular Cytosol: Escaping from the Endolysosomal System. *Integr. Biol.* **2010**, *2*, 265–277.
27. Janib, S. M.; Moses, A. S.; MacKay, J. A. Imaging and Drug Delivery Using Theranostic Nanoparticles. *Adv. Drug Delivery Rev.* **2010**, *62*, 1052–1063.
28. Park, K.; Lee, S.; Kang, E.; Kim, K.; Choi, K.; Kwon, I. C. New Generation of Multifunctional Nanoparticles for Cancer Imaging and therapy. *Adv. Funct. Mater.* **2009**, *19*, 1553–1566.